Int. J. Appl. Ceram. Technol., 1–11 (2014)
DOI:10.1111/ijac.12301

Effect of Electrodeposition Parameters on the Microstructure and Corrosion Behavior of DCPD Coatings on Biodegradable Mg–Ca–Zn Alloy

Hamid Reza Bakhsheshi-Rad,* Esah Hamzah, and Safaa N. Saud

Department of Materials, Manufacturing and Industrial Engineering, Faculty of Mechanical Engineering, Universiti Teknologi Malaysia, 81310, Johor Bahru, Johor, Malaysia

Mamoun Medraj

Department of Mechanical Engineering, Concordia University, 1455 De Maisonneuve Blvd. West, Montreal, QC, H3G 1M8, Canada

In this study, DCPD (Brushite, $CaHPO_4.2H_2O$) coatings were prepared on the surface of a Mg–Ca–Zn alloy using different current density (0.15–1.2 mA/cm^2) and deposition time (5–90 min). The results revealed that DCPD with needle-like morphology was observed for the current density between 0.15 and 0.4 mA/cm^2, whereas plate-like morphology was obtained at current density above 0.8 mA/cm^2. The results showed that surface roughness increased with increasing current density. The lowest corrosion rate of 0.14 mm/year was obtained for the dense and uniform DCPD coating at 0.4 mA/cm^2, while further increase has deleterious effect on the corrosion resistance.

Introduction

Mg and its alloy are receiving great attention as biodegradable materials for implant application particularly as a temporary stent. Due to Mg, alloys can be dissolved and absorbed in the human body and do not require second surgical procedure for implant removal.[1,2] Mg alloys also have similar mechanical properties to natural bone, good biological performance, and biodegradability in the physiological environment.[3,4] However, the main obstacle to the use of Mg alloys is their high electrochemical activity and hence fast corrosion rate.[1,5] Thus, the corrosion rate of Mg alloys must be controlled for its feasible use as implant materials.[1,6] To achieve this aim, calcium phosphates (Ca-P) are extensively used for coating of Mg alloys to slow down its corrosion rate.[1,6,7] Different kinds of the Ca-P, such as monocalcium phosphate monohydrate, dicalcium phosphate dihydrate, hydroxyapatite, and tricalcium phosphate, were used as coating materials.[6,7] Among these, hydroxyapatite (HA, $Ca_{10}(PO_4)_6(OH)_2$) is the most fascinating form of Ca-P due to the its excellent biocompatibility, bioaffinity, and osseoconductivity.[8,9] HA also has similar chemical and biological properties to human hard tissues as well as HA coating improved corrosion resistance of Mg alloys in biological environment by providing barrier film on the alloy surface.[10–13] However, the synthesis of HA via precipitation method leads to the formation of agglomerate crystals whose size is often difficult to control.[6] Using DCPD ($CaHPO_4.2H_2O$) as a precursor, it is feasible to control the crystal size of DCPD and subsequently convert it directly to HA.[7] DCPD is frequently applied as the initial component of bone cements, and it is a promising coating for clinical use.[7] DCPD is also biocompatible with different cell lines such as murine fibroblast cells.[7,12] Different methods [1,2,5,10] such as fluoride conversion coating, polymer coating, hot spraying, phosphating treatment, laser cladding, and electrodeposition were investigated to improve the corrosion resistance of Mg alloys. Among these techniques, electrodeposition used as a process having low temperature, low cost, ability to deposit on complex shapes materials, and simple control of parameter.[14] Hu *et al.*[14] investigated the electrochemical deposition behavior of calcium phosphate (Ca-P) coating at different current densities (0.25–1.75 mA/cm^2) for 1 h. Djosic *et al.*[15] studied calcium phosphate coating at different current densities (5–10 mA/cm^2) and various times (1–30 min). However, Wang *et al.*[16] studied calcium phosphate coating on Ti alloy by electrochemical deposition method at various voltages (4–10 V) for different times (20–120 min). In this regard, Jamesh *et al.*[17] investigated electrodeposition of Ca-P coating on Mg alloy at 100 mV. Other researcher [18–20] coated Ca-P on

*rezabakhsheshi@gmail.com; bhamidreza2@live.utm.my

Mg alloy at current density between 0.4 and 0.5 mA/cm^2 for 1 h. As mentioned, several studied [6,7,14] were reported on the fabricating of Ca-P coating on Mg and Ti alloy, but the mechanism of electrodeposition of DCPD onto Mg alloys has not been entirely clarified. Therefore, in this research, DCPD coatings at various current densities (0.15–1.2 mA/cm^2) and deposition time (5–90 min) were applied, and their effects on the microstructure and corrosion behavior of Mg–Zn–Ca alloy were investigated.

Materials and Methods

Pure magnesium ingot (99.98 wt%, Fushun Aluminium Alloy Company, China), high purity Zn chip (99.999 wt%, National Chemical Reagent Company, Shenyang, China), and Mg–32 wt% Ca master (98 wt%, Shanghai ruizheng chemical technology, Shanghai, China) were used to prepare magnesium alloys. The melting was conducted in an electronic resistance furnace under argon gas in a mild steel crucible coated with boron nitride. The melting temperature was set at 760°C for 45 min. The first 30 min was for melting, and the remaining 15 min for complete melt homogenization. Then, the melt with a constant concentration of Ca (0.5 wt%) and Zn (3 wt%) was cast into a 300°C preheated stainless steel mold to obtain ingots and specimens test for microstructural observation.[21] Specimens 10 × 10 × 5 mm in size were prepared from the as-cast alloys ingots, and the samples were then mechanically wet-ground for microstructural observation. DCPD coating was produced via electrodeposition at 70°C for different deposition duration between 5 and 90 min. A conventional cell was fitted with a graphite rod as the anode and the Mg–Ca–Zn sheet (10 × 10 × 5 mm) as the cathode. Saturated calomel electrode (SCE) served as a reference electrode along with a potentiostat/galvanostat instrument for electrochemical measurements. For preparing DCPD on Mg alloy, the current density was varied between 0.15 and 1.2 mA/cm^2. The solution concentration was kept uniform using a magnetic stirrer controlled at 120 rpm. The electrolyte was prepared by dissolution of $Ca(NO_3)_2$ (0.042 mol/L), $NH_4H_2PO_4$ (0.025 mol/L), $NaNO_3$ (0.1 mol/L), and H_2O_2 (10 mol/L) at pH 5 in room temperature. Each experiment was repeated twice to check the reproducibility of the results. Microstructure observation was performed using a scanning electron microscope (SEM; JEOL JSM-6380LA, Tokyo, Japan) equipped with Oxford energy dispersive X-ray spectrometer (EDS) analysis with an operating voltage of 20 kV and transmission electron microscope (TEM HT7700; Hitachi, Tokyo, Japan). An X-ray diffractometer (XRD; Siemens-D5000, Munich, Germany) was used to evaluate the phase transformation and crystallite size of the specimens using Cu-Kα radiation (λ = 1.5405 Å) generated at 35 kV and 25 mA operated at the step size of 0.02° and scan speed of 2° min^{-1}. Electrochemical polarization test was carried out using PARSTAT 2263 potentiostat/galvanostat (Princeton Applied Research, Oak Ridge, TN) advanced electrochemical system. The surface topography of the coated and uncoated specimens was evaluated using atomic-force microscopy (AFM; NanoScope IV, Digital Instruments). AFM imaging was performed in the tapping mode at room temperature using a standard silicon nitride probe with a spring constant of 0.58 N/m and a typical radius of 10 nm. The scanning area selected was 10 × 10 μm. Fourier-transform infrared (FTIR; ALPHA-T, Bruker, Ettlingen, Germany) spectroscopy was used to determine the surface functional groups of the coated sample. All the spectra in these experiments were obtained by adding 64 interferograms at a resolution of 8 cm^{-1} in the spectral range of 3950–450 cm^{-1}. The bonding strength of the coated specimens was measured according to ASTM F1044 standard using universal testing machine (Instron 5569, Norwood, MA). Rectangular specimens with the dimensions of 30 ×10 mm were prepared. The cross-head displacement rate was 1 mm/min with a 10 kN load cell. Three coated specimens were tested, and the average value was reported. Electrochemical cell consisted of the sample as working electrode, a saturated calomel electrode (SCE) as reference electrode, and a platinum rod as counter electrode. Each sample was masked by paraffin wax such that a surface area of 1.0 × 1.0 cm^2 with a scan rate of 0.5 mV/s initiated at −250 mV below the open-circuit potential. The test was conducted at 37°C in an open air glass cell containing 350 mL Kokubo solution at pH 7.66. The simulated body fluid (SBF) was prepared according to the previously reported method.[22]

Result and Discussion

Figure 1a shows the influence of the applied current densities (0.15–1.2 mA/cm^2) on the mass of calcium phosphate at various deposition times (5–90 min). Increasing applied current density up to 0.4 mA/cm^2 lead to significant increase in the weight of the deposition due to more ions reached to the cathode surface; hence, the coating mass increased in the duration between 5 and 60 min. However, a further increase in the current density up to 1.2 mA/cm^2 resulted in a less

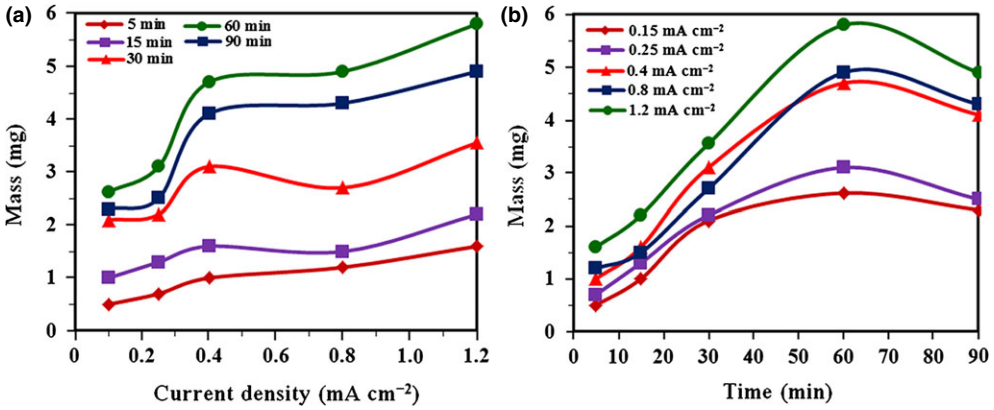

Fig. 1. (a) Effect of current densities on deposit weight of DCPD for different deposition times and (b) effect of deposition times on deposit weight of DCPD for different current densities.

significant increase in mass gain. When current density amplifies, the rate of H_2 generation increased on the surface of cathode, which leads to more hydrogen bubbles accumulating on the cathode surface. This phenomenon caused decrease in phosphate precipitation on the cathode surface.[15,23]

Figure 1b shows the influence of the electrodeposition time on the mass of calcium phosphate at different current density (0.15–1.2 mA/cm^2). As the deposition time increased to 30 min, the mass of coating increased to 3.1 mg when the current density increased from 0.15 to 0.4 mA/cm^2. For current density at 0.4 mA/cm^{2,} as the deposition time increases to 60 min, the coating mass significantly increased to 4.7 mg due to high reaction rate. However, further increase in deposition time to 90 min leads to weight of the deposition decreases to 4.1 mg due to generation of large amount H_2 on the surface of cathode which resulted in accumulation of hydrogen bubbles on the surface of cathode and thus preventing the formation of phosphate on the cathode surface.[15] The depletion of the coating film via H_2 generation could be another reason of deposit weight loss. However, the weight gain of the deposition could be attributed to the phosphate deposition and its growth, in addition to the electrochemical reaction of H_2 generation. Higher current density accompanied by further increase in deposition time to 60 min leads to an increase in mass deposition. H_2 bubbles are accelerated at higher current densities leading to the faster release of fresh parts of the cathode surface than at lower current density resulting in more deposition.[15,23] The highest mass gain was obtained by deposition at 60 min due to the deposition of coarse particle on the cathode surface. However, further increase to 90 min resulted in more coarse particle depositing on the surface, which caused some of the coarse particles to fall off from the coating thus decreasing the mass. This decrease also could be attributed to the damage caused by the fast evolving hydrogen bubbles. This is in accord with the results of Djosic *et al.*[15] The formation mechanism of DCPD coatings can be seen in the Fig. 2 which includes the precipitation reaction and the crystallization process. The hydrogen evolution from water molecules occurred near the substrate through reaction reported at,[12] and its concentration increases rapidly around cathode surface (Fig. 2a). These hydroxide ions produced via the electrochemical process lead to an increase in the pH value in the vicinity of the cathode according to the reaction reported at.[12] The suitable local chemical environment in the vicinity of the cathode provided the HPO_4^{2-} due to high pH value of the electrolyte which subsequently combined with Ca^{2+} to produce a

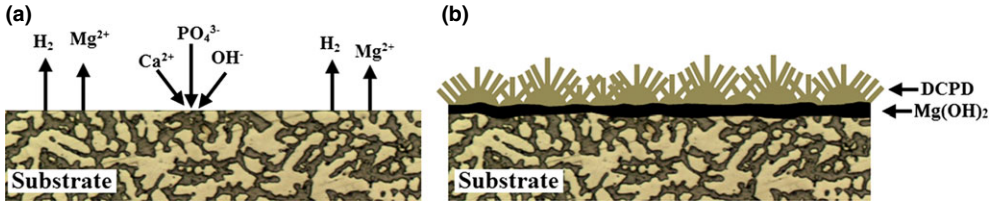

Fig. 2. Schematic illustration of the formation mechanism of DCPD coating on Mg–Zn–Ca alloy.

DCPD which precipitated on the surface of the substrate through reaction reported at.[12] In addition, insoluble $Mg(OH)_2$ film formed due to readily reaction of Mg with OH (Eq. 1) at the interface DCPD coating with the Mg–Zn–Ca alloy substrate. With increasing current density to 1.2 mA/cm^{2,} more DCPD will be formed on the surface of the alloy (Fig. 2b).

$$Mg + 2H_2O \rightarrow Mg(OH)_2 \downarrow + H_2 \uparrow \qquad (1)$$

Figure 3 exhibits the surface morphology of the Mg–Ca–Zn alloy before coating process. A typical cast structure consisted of α-Mg grains accompanied by a number of intermetallic particles distributed mainly along grain boundaries. Only secondary phases were found in the grain boundary and the interdendrite in matrix. The EDS result shows that the secondary phase was composed of Ca, Zn, and Mg indicating the formation of $Ca_2Mg_6Zn_3$. Figure 4 shows the SEM micrographs of the calcium phosphate coating specimens at constant deposition duration of 60 min for different current densities (0.15–1.2 mA/cm^2). It can be observed that the DCPD with needle-like morphology (rosette pattern) almost covered the entire surface of Mg–Ca–Zn alloy due to the lower current density of 0.15 mA/cm^2 which leads to the slow growth rate of deposited films (Figs. 4a and b). This can be attributed to the smaller deposited particles at lower current density. The DCPD morphology of the specimen at a current density of 0.25 mA/cm^2 shows the growth of the crystal toward the outside, and the length of needle significantly increased to 5 μm as shown in Figs. 4c and d. A further increase in the current density to 0.4 mA/cm^2 leads to the appearance of stacks of rosette pattern with almost uniform and upright structure as shown in Figs. 4e and f. At the current density of 0.8 mA/cm^2, the DCPD with plate-like morphology, having precipitates stacking loosely with each other on the alloy surface as can be seen in Figs. 4g and h. In this case, needle forms of the DCPD crystals appeared between the wide DCPD plates. The width of a platelet is around 10 μm. The volcano-like site also can be observed on the deposited film due to the evolution of high amount of H_2 bubbles on the surface of the cathode. The volcanoes have a round shape, suggesting that the DCPD phase formed around the gas bubble.[23] However, at higher current density (1.2 mA/cm^2), deposits showed nonuniform distribution of DCPD phase with plate-like morphology as can be seen in Figs. 4j and k. EDS analysis showed that with increasing current density, the Ca/P atomic ratio increased. At the area A, B, and C shown on the micrographs of Fig. 5, the Ca/P atomic ratio of DCPD was about 1.13, 1.25, and 1.37, respectively. However, Ca/P atomic ratios at area D was 1.49 indicating the high amount of HA deposited on the cathode surface.

Figure 6 shows cross-sectional SEM image of the DCPD-coated specimen at two different current densities, indicating dense coating with relatively uniform thickness (15–20 μm) indicates that the coating can be tightly adhered to the substrate. However, there are some cracks coated at 0.8 mA/cm^2, but they are not entirely transverse in the coating. Figure 7 shows the TEM image and related selected area diffraction patterns (SADP) of the DCPD coatings scraped by a sharp instrument at different current densities. It was found that the DCPD crystals have a lath-like shape with 150–300 nm width and 700 nm/μm length in the range of 0.25–1.2 mA/cm^2 as can be seen in Figs. 7a–d. The DCPD crystal size increased with increasing the current density. The diffraction of DCPD nanosized crystallites, presented in the insets of Fig. 7, shows a continuous ring patterns with no d-spacing of HA.

The XRD patterns of uncoated and deposited coatings at constant deposition duration of 60 min for

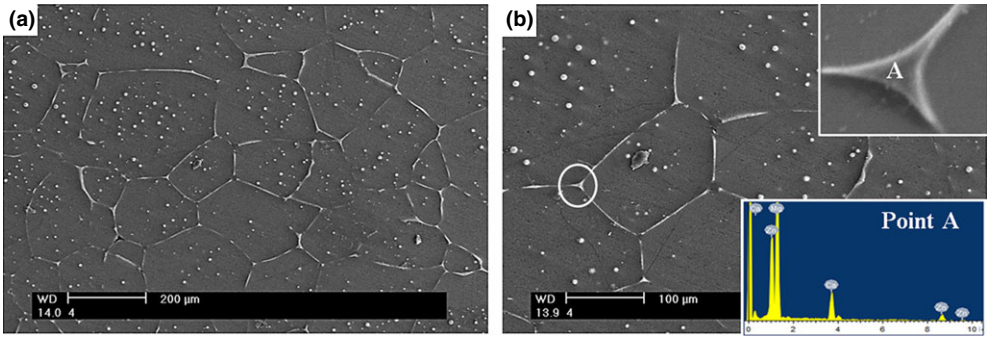

Fig. 3. Surface morphology of the Mg–Ca–Zn alloy before coating process; (a) low magnification and (b) high magnification.

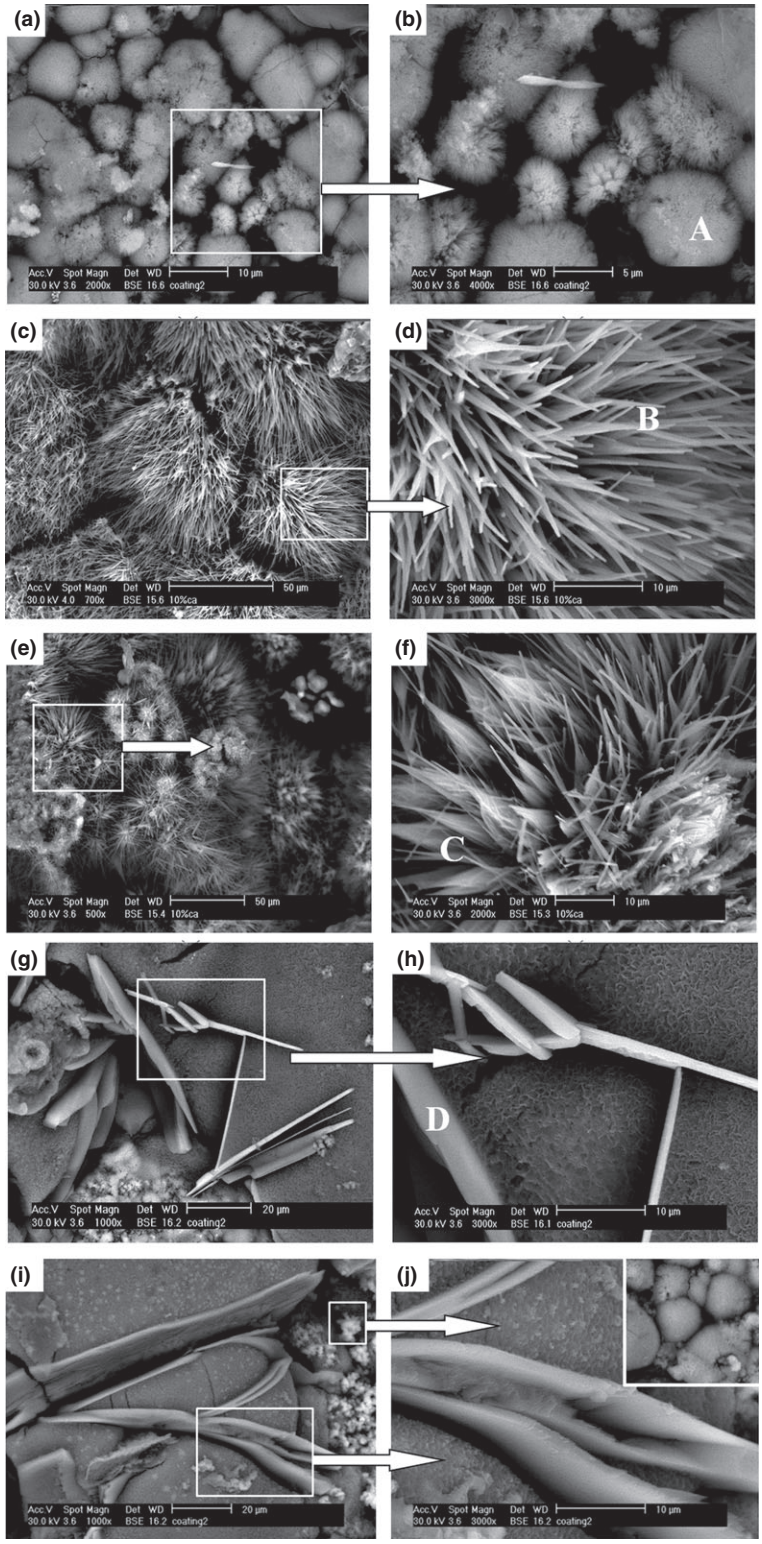

Fig. 4. SEM micrographs of DCPD coating at 60 min for different current densities: (a, b) 0.15 mA/cm^2, (c, d) 0.25 mA/cm^2, (e, f) 0.4 mA/cm^2, (g, h) 0.8 mA/cm^2, and (j, k) 1.2 mA/cm^2.

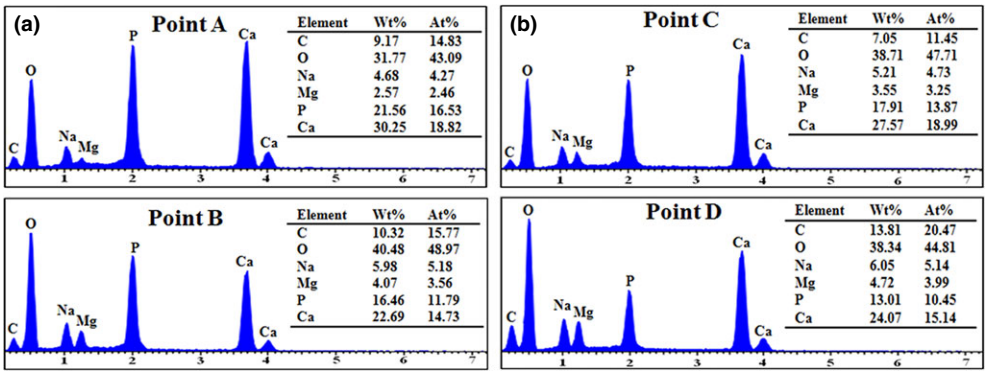

Fig. 5. EDX analysis of (a) point A, B and (b) point C, D.

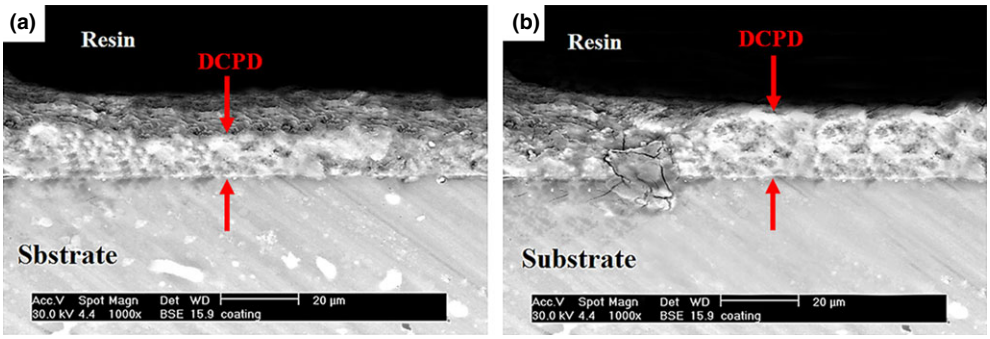

Fig. 6. Cross-sectional SEM image of DCPD for different current densities (a) 0.25 mA/cm^2 and (b) 0.8 mA/cm^2.

various current densities from 0.15 to 1.2 mA/cm^2 are shown in Fig. 8. The XRD pattern of uncoated Mg–Ca–Zn alloy specimens shows the presence of relatively small, although discernible, reflections of $Ca_2Mg_6Zn_3$ phases (JCPDS file no. 12-0266) accompanied with α-Mg (JCPDS file no. 65-3365) reflection. The $Ca_2Mg_6Zn_3$ phase has a trigonal structure with the space group P31c and the lattice parameters a = 50.97 nm, c = 51.0 nm.[24] XRD pattern of calcium phosphate coating shows the presence of DCPD (JCPDS file no. 09-0077) and Mg as main phases, accompanied with trace amount of HA (JCPDS file no. 09-0432).[25] As it can be seen that by increasing current densities from 0.15 to 1.2 mA/cm^2, the phase type DCPD and HA were not changed, but their peaks intensity changed (Fig. 8a). A peak of DCPD at 32° increased with the increase of current density. The peak associated to HA at 26° increased up to 0.4 mA/cm^2 and then decreased. The increase in HA intensity can be attributed to the enhancement of HA phase crystallinity with increasing current density. The XRD patterns of the coating at various duration from 5 to 90 min indicated that a peak of DCPD at 25° increased with the time, while the intensity of peaks of HA became broader. The Mg matrix also decreases with the increasing deposition time as seen in Fig. 8b. This was related to the increasing film thickness with increasing deposition time. The peaks of HA became broader with increasing deposition time indicating a formation of film with poor crystallinity, or it consisted of small crystallites, which is similar to natural bone mineral, favorable for tissue compatibility.[23,26] It is also observed that the diffraction peak intensities of the HA phases for longer deposition time are considerably higher compared to the shorter time indicating more formation of HA with deposition time.

The FTIR spectra of DCPD detached from the specimens coated at different current densities are shown in Fig. 9. It can be seen that the absorption band at about 3436 cm^{-1} and another strong band at 1654 cm^{-1} is due to O–H stretching vibration which indicates the presence of water molecules in the DCPD structure, while the absorption band at 1414 cm^{-1} is attributed to the vibration HCO^{-3} group of DCPD. Numerous water molecules existed between the individual $Ca_9(PO_4)_6$ clusters in the spherical structure of the amorphous precursor.[26] The vibrations band related to

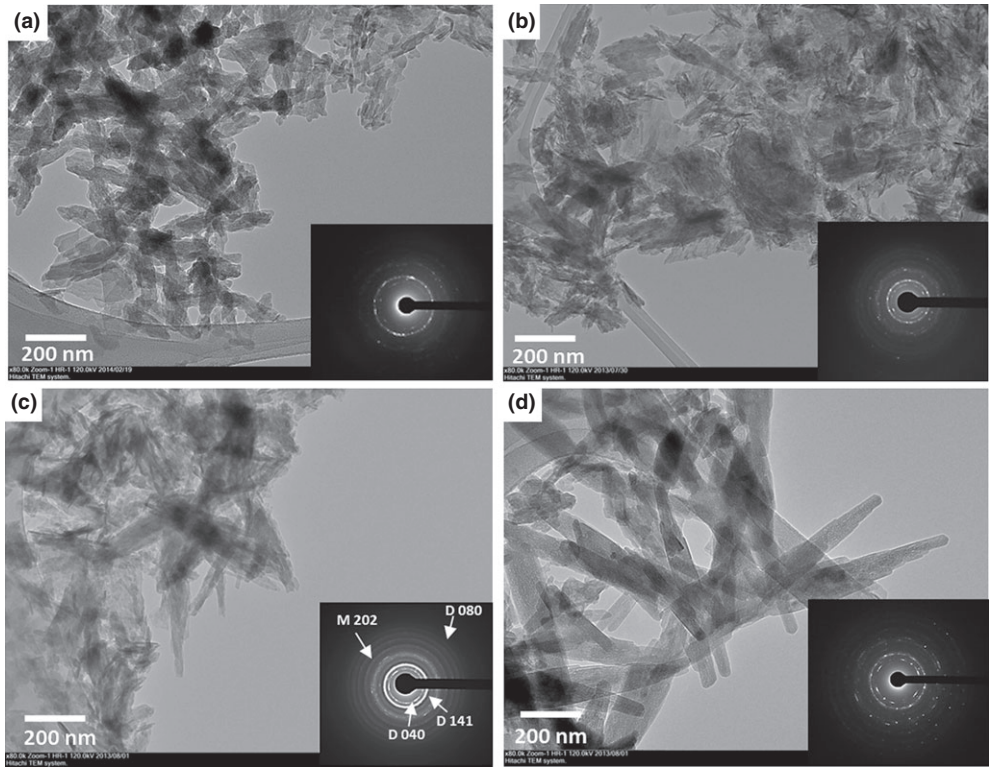

Fig. 7. TEM micrographs with selected area diffraction pattern of DCPD coating at 60 min for different current densities: (a) 0.25 mA/cm^2, (b) 0.4 mA/cm^2, (c) 0.8 mA/cm^2, and (d) 1.2 mA/cm^2.

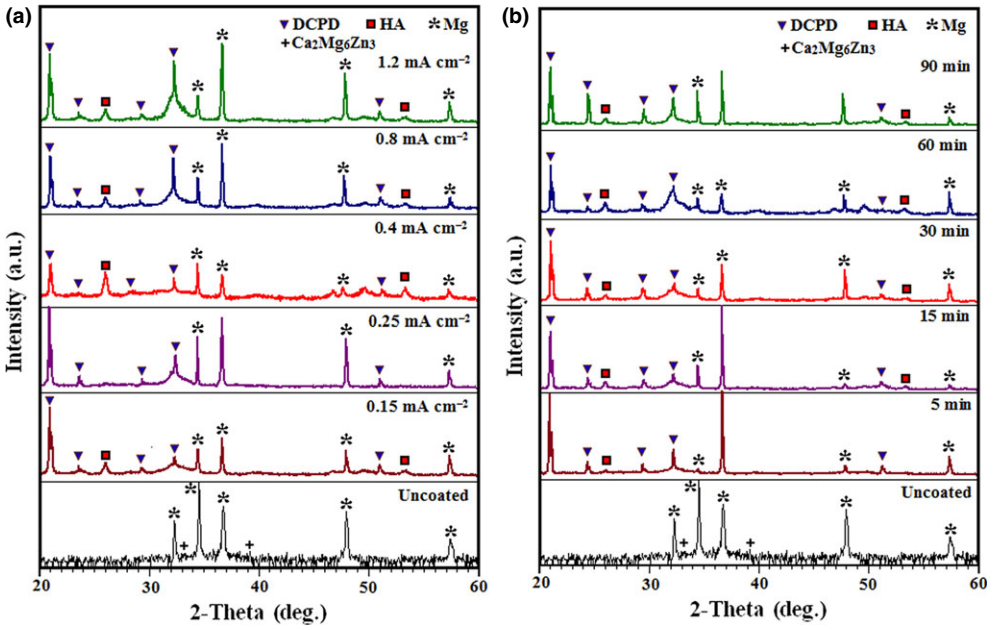

Fig. 8. X-ray diffraction patterns of uncoated and DCPD coating (a) at 60 min for different current densities and (b) at 0.4 mA/cm^2 for different deposition times.

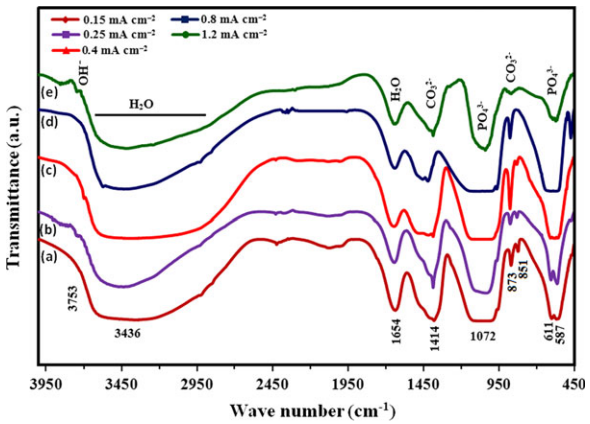

Fig. 9. The FTIR characteristic bands of DCPD coating at 60 min for different current densities: (a) 0.15 mA/cm^2, (b) 0.25 mA/cm^2, (c) 0.4 mA/cm^2, (d) 0.8 mA/cm^2, and (e) 1.2 mA/cm^2.

PO_4^{3-} ion are observed at 587 cm^{-1} (v_4), 611 cm^{-1} (v_4), and 1072 cm^{-1} (v_3). The occurrence of phosphate vibrations may confirm the transformation of the amorphous phase into the crystalline phase. This result was in accord with previous published work.[26] The strong band at 1414 cm^{-1} showed the incorporation of the carbonate group into the DCPD lattice.

The peaks around to 2450 cm^{-1} are related to KBr. Furthermore, carbonate can be formed by the reaction of hydroxyl ions (OH^-) with carbon dioxide attained by the air within drying process. Although the applied current did not cause significant change in the crystal structure of DCPD, noticeable change occurred to the microstructure that could be observed in the SEM micrographs as shown in Fig. 4. The surface topography of the uncoated and DCPD-coated specimens at different current densities (0.15 to 0.8 mA/cm^2) for constant deposition duration of 60 min are shown in Fig. 10. The bare Mg alloy had surface roughness average (R_a) and root mean square (RMS) values of 199 and 234 nm, respectively (Figs. 10a and f). It is evident that the coatings deposited at a current density of 0.15 mA/cm^2 were about 310 nm as can be seen in Fig. 10b. A further increased in current density to 0.4 mA/cm^2 resulted in an increase in the coating roughness (R_a = 350 nm) as shown in Fig. 10c. At higher than 0.4 mA/cm^2 current density, the coating roughness (R_a) significantly increased (580 nm) as can be seen in Figs. 10d and e. The graph shows both R_a and RMS increased with increasing current densities from 0.15 to 0.8 mA/cm^2 (Fig. 10f). This is due to the higher rate of H_2 generation from the cathode surface resulting in more porosity in the coating. Besides, at a high value of current density, the rate of deposition increased significantly, and coarse particles were deposited, contribution to the increase in coating roughness. In addition, the electric field-induced particle aggregation and sedimentation decrease the amount of fine particles in the suspension and in the deposit which leads to more amounts of coarse particles deposited on the coating layer, and thus, the rougher surface was obtained.[27] At higher applied current density, this phenomenon was more pronounced, which caused some coarse particles to fall off from the coating and produced nonuniform deposit film. This result is in good agreement with a published work by Djosic *et al.*[15] As the deposition kinetic improved as a result of high current density, the fast deposition of particles prevented the formation of a uniform coating layer and therefore large pores formed in the deposited film with high surface roughness. The bonding strength of the coating at 0.15, 0.25, and 0.4 mA/cm^2 was around 16.4, 15.7, and 15.3 MPa, respectively, which is in accordance with required norms (15 MPa) in orthopedic implant industry.[11] However, bonding strength of coated specimens at 0.8 and 1.2 mA/cm^2 was around 14.6 and 12.2 MPa, respectively. The lower bonding strength of coated specimens at higher current densities can be due to deposition of more coarse particle on the surface and more hydrogen bubbles accumulating on the specimens surface which cause poor bonding between the coating and substrate.

Figure 11 exhibited the polarization curves recorded after 1 h of exposure to Kokubo solution for uncoated and DCPD-coated specimens at different applied current densities from 0.5 to 1.2 mA/cm^2. The DCPD-coated specimens at various current density presented lower corrosion current density and nobler potential compared to the uncoated specimen indicating lower corrosion rate of the coated alloys. This is due to formation of DCPD as a protective layer on the surface of Mg alloy which blocked the reaction for transportation of species (such as water and chlorine) hence increasing the corrosion resistance of the coated samples.[28,29] Among the five DCPD-coated specimens at different current densities, that coated at 0.4 mA/cm^2 presented the lowest corrosion current density (6.12 μA/cm^2), while that coated at 0.15 mA/cm^2 indicated the highest corrosion current density (59.8 μA/cm^2). These values were followed by the 0.8 mA/cm^2 coated sample (9.15 μA/cm^2) and 1.2 mA/cm^2 coated sample (27.4 μA/cm^2), indicating that the corrosion behavior of the coated alloy is significantly affected by the applied coating current densities. As can be seen, coated alloy at 0.4 mA/cm^2 exhibited the more positive corrosion potential (−1602.5 mV_{SCE}) than the coated

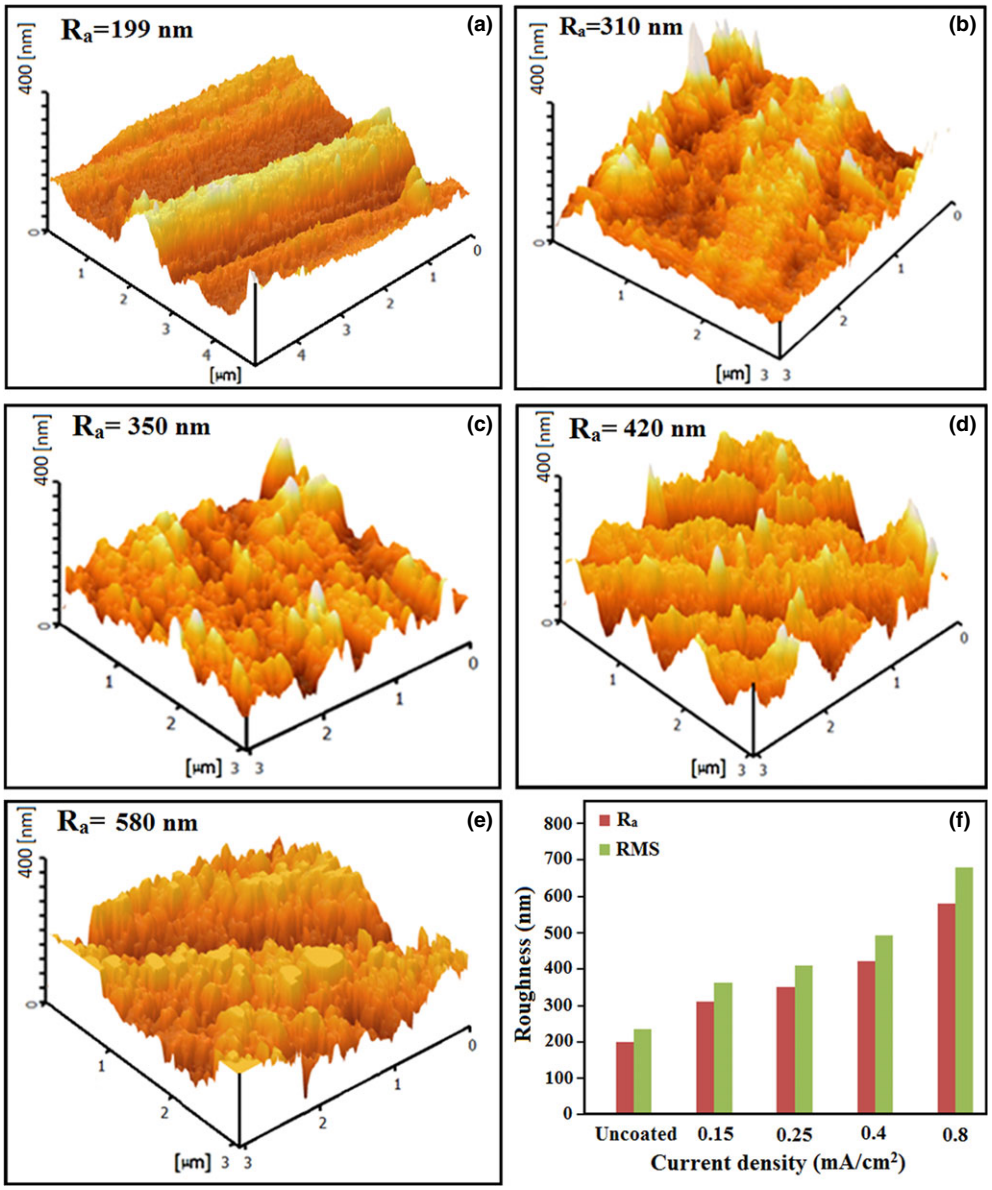

Fig. 10. AFM topography of (a) uncoated and (b) DCPD coating at 60 min for different current densities: 0.15 mA/cm^2, (c) 0.4 mA/cm^2, (d) 0.8 mA/cm^2, (e) 1.2 mA/cm^2, and (f) surface roughness of uncoated and DCPD coated for different current densities.

alloy at 0.8 mA/cm^2 (−1612.9 mV_{SCE}) and 1.2 mA/cm^2 (−1622.2 mV_{SCE}). This is attributed to the observation that increasing current density higher than 0.4 mA/cm^2 led to more generation of H_2 from the cathode surface which resulted in more porosity in the deposited coatings.

Electrochemical parameters of uncoated alloy in comparison with DCPD-coated specimens at various current densities are presented in Table I. The corrosion rate (P_i) of samples obtained from the corrosion current density was measured according to the following equation:[12,30,31]

$$P_i = 22.85 i_{corr} \quad (2)$$

According to the Eq. (2), coated alloy using 0.8 and 1.2 mA/cm^2 showed similar corrosion rate in the range of 0.21–0.63 mm/year. However, the coated alloy using 0.4 mA/cm^2 showed the lowest corrosion rate. Also, from the electrochemical parameters (i_{corr}, β_a, and β_c) of specimens, the polarization

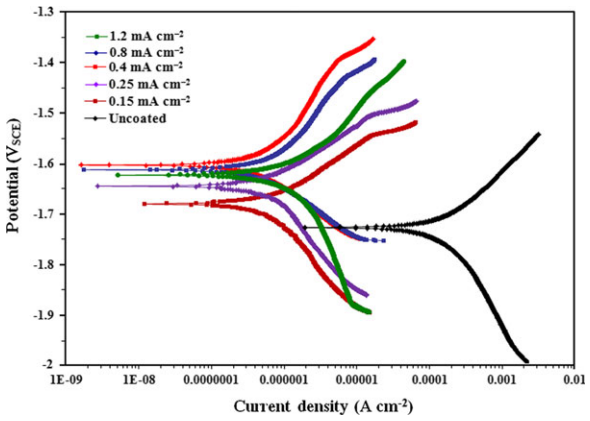

Fig. 11. Potentiodynamic polarization curves of uncoated and DCPD coated at 60 min for different current densities in Kokubo solution.

resistance (R_P) was calculated according following equation:[22,32–34]

$$R_P = \frac{\beta_a \beta_c}{2.3(\beta_a + \beta_c) i_{corr}}, \quad (3)$$

where β_a is the anodic Tafel slopes, β_c is the cathodic Tafel slopes, and i_{corr} is the corrosion current density. The corrosion behavior of the DCPD-coated specimen enhanced as R_P values increased with increasing current density up to 0.4 mA/cm^2, while further increase in current density to 1.2 mA/cm^2 decreased the polarization resistance. The coated alloy using 0.15 mA/cm^2 presented the lowest polarization resistance (0.46 kΩcm^2), while coated alloy using 0.4 mA/cm^2 showed the highest polarization resistance (3.30 kΩcm^2) which further confirmed the results of corrosion rate. DCPD-coated alloy presented variation of the corrosion rates which is due to the variation in the microstructure (coating morphology) of the specimens at various current densities. The coated alloy using 0.15 mA/cm^2 presented the highest corrosion rate which is attributed to its thin coating layer. As expected, it was observed that higher coating thickness resulted in higher protection and lower corrosion rate in the SBF solution.[35,36] The integrity of the coating layer is the other factor that has significant effect on the corrosion resistance of the alloy. The coated alloy using 0.4 mA/cm^2 showed best corrosion resistance compared to the coated alloy using 0.8 and 1.2 mA/cm^2 even with thinner coating layer due to an existence of less amount of porosity and microvoids in the coating layer due to better shielding of the substrate from the corrosive medium of SBF solution.

Conclusion

In this study, DCPD coating using different current density from 0.15 to 1.2 mA/cm^2 and deposition time from 5 to 90 min was fabricated on the surface of 96.5Mg-0.5Ca-3Zn wt% alloy. The result revealed that the highest deposited mass was obtained for the deposition time of 60 min. Increasing the applied coating current density resulted in increasing the mass gain, but higher than 0.4 mA/cm^2 current density has less significant effect on the coating mass. The AFM and TEM results showed that roughness and crystal size of DCPD increases with increasing applied coating current density. The morphology of DCPD deposited at lower current densities was needle-like, while plate-like morphology was deposited at higher current densities. The Ca/P atomic ratio increased from 1.13 to 1.49 with increasing current density, indicating the increased deposition of HA on the cathode surface. Polarization test showed that the corrosion rates of the DCPD-coated sample using 0.4 mA/cm^2 was lower compared to the samples coated at higher applied current density. The DCPD coating at 0.4 mA/cm^2 for 60 min exhibited uniform and com-

Table I. Electrochemical Parameters of Uncoated and DCPD Coated at 60 min for Different Current Densities in Kokubo Solution Attained from the Polarization Test

Alloy	Corrosion potential, E_{corr} (mV vs SCE)	Current density, i_{corr} (μA/cm^2)	Cathodic slope, β_c (mV/decade) vs SCE	Anodic slope β_a (mV/decade) vs SCE	Polarization resistance, R_P (kΩcm^2)	Corrosion rate, P_i (mm/year)
Mg-0.5Ca-3Zn	−1726.7 ± 18	236.4 ± 10	298 ± 9	135 ± 5	1.7 ± 0.33	5.40 ± 0.17
DCPD-0.15 mA/cm^2	−1679.9 ± 17	59.8 ± 4	187 ± 8	95 ± 4	4.6 ± 0.11	1.36 ± 0.11
DCPD-0.25 mA/cm^2	−1644.4 ± 16	43.1 ± 2	242 ± 12	78 ± 3	5.9 ± 0.13	0.98 ± 0.13
DCPD-0.4 mA/cm^2	−1602.5 ± 19	6.12 ± 0.1	332 ± 13	54 ± 4	33.0 ± 0.07	0.14 ± 0.04
DCPD-0.8 mA/cm^2	−1612.9 ± 15	9.15 ± 0.2	310 ± 15	63 ± 2	24.9 ± 0.09	0.21 ± 0.06
DCPD-1.2 mA/cm^2	−1622.2 ± 16	27.4 ± 0.8	287 ± 14	72 ± 3	9.1 ± 0.08	0.63 ± 0.09

pact film with needle-like morphology offering highest corrosion resistance.

Acknowledgments

The authors would like to acknowledge the Universiti Teknologi Malaysia (UTM) and Nippon Sheet Glass Foundation for providing research facilities and financial support under Grant No. R.J.130000.7324.4B136.

References

1. X. N. Gu, N. Li, W. R. Zhou, Y. F. Zheng, and X. Zhao, *Acta Biomater.*, 7 1880–1889 (2011).
2. L. H. Li, *et al.*, *Surf. Interface Anal.*, 46 7–15 (2014).
3. Z. Wei, H. Du, and E. Zhang, *Surf. Interface Anal.*, 43 791–794 (2011).
4. H. Cao and X. Liu, *Int. J. Appl. Ceram. Technol.*, 10 1–10 (2013).
5. R. Amini and A. A. Sarabi, *Appl. Surf. Sci.*, 257 7134–7139 (2011).
6. Y. Shi, M. Qi, Y. Chen, and P. Shi, *Mater. Lett.*, 65 2201–2204 (2011).
7. S. Shadanbaz and G. J. Dias, *Acta Biomater.*, 8 20–30 (2012).
8. H. R. Bakhsheshi-Rad, E. Hamzah, M. Daroonparvar, R. E. Kahrizsangi, and M. Medraj, *Ceram. Int.*, 40 7971–7982 (2014).
9. H. Farnoush, J. A. Mohandesi, and D. H. Fatmehsari, *Int. J. Appl. Ceram. Technol.*, 10 87–96 (2013).
10. E. A. Abdel-Aal, D. Dietrich, S. Steinhaeuser, and B. Wielage, *Surf. Coat. Technol.*, 202 5895–5900 (2008).
11. M. Esnaashary, M. Fathi, and M. Ahmadian, *Int. J. Appl. Ceram. Technol.*, 11 47–56 (2014).
12. H. R. Bakhsheshi-Rad, M. H. Idris, and M. R. Abdul-Kadir, *Surf. Coat. Technol.*, 222 79–89 (2013).
13. A. Dey, *Int. J. Appl. Ceram. Technol.*, 11 65–82 (2014).
14. R. Hu, C. Lin, H. Shi, and H. Wang, *Mater. Chem. Phys.*, 115 718–723 (2009).
15. M. S. Djosic, V. Panic, J. Stojanovic, M. Mitric, and V. B. Mi˘skovi′c-Stankovic, *Colloids Surf. A Physicochem. Eng. Asp.*, 400 36–43 (2012).
16. M. C. Wang, W. J. Shih, K. M. Chang, S. H. Wang, W. L. Li, and H. H. Huang, *J. Non-Cryst. Solids*, 356 1546–1553 (2010).
17. M. Jamesh, K. Satendra, and T. S. N. S. Narayanan, *J. Coating. Tech. Res*, 9 495–502 (2012).
18. C. Wen, S. Guan, L. Peng, C. Ren, X. Wang, and Z. Hu, *Appl. Surf. Sci.*, 255 6433–6438 (2009).
19. Y. Song, S. Zhang, J. Li, C. Zhao, and X. Zhang, *Acta Biomater.*, 6 1736–1742 (2010).
20. J. Li, Y. Song, and S. Zhang, *Biomaterials*, 31 5782–5788 (2010).
21. Y. Li, *et al.*, *Acta Biomater.*, 8 3177–3188 (2012).
22. H. R. Bakhsheshi-Rad, *et al.*, *Mater. Design*, 53 283–292 (2014).
23. S. H. Wang, W. J. Shih, and W. L. Li, *J. Eur. Ceram. Soc.*, 25 3287–3292 (2005).
24. P. M. Jardim, G. Solórzano, and J. B. Vander Sande, *Microsc. Microanal.*, 8 487–496 (2002).
25. H. Wang, S. Zhu, L. Wang, Y. Feng, X. Ma, and S. Guan, *Appl. Surf. Sci.*, 307 92–100 (2014).
26. S. Rössler, A. Sewing, M. Stölzel, R. Born, D. Scharnweber, M. Dard, and H. Worch, *J. Biomed. Mater. Res. A*, 64 655–663 (2003).
27. I. Zhitomirsky, *Mater. Lett.*, 42 262–271 (2000).
28. W. Zhou, D. Shan, E. H. Han, and W. Ke, *Corros. Sci.*, 50 329–337 (2008).
29. H. R. Bakhsheshi-Rad, E. Hamzah, M. Daroonparvar, M. Kasiri-Asgarani, and M. Medraj, *Ceram. Int.*, 40 7971–7982 (2014).
30. Z. Shi, M. Liu, and A. Atrens, *Corros. Sci.*, 52 579–588 (2010).
31. Z. Shi and A. Atrens, *Corros. Sci.*, 53 226–246 (2011).
32. G. R. Argade, K. Kandasamy, S. K. Panigrahi, and R. S. Mishra, *Corros. Sci.*, 58 321–326 (2012).
33. M. Liu, P. Schmutz, P. J. Uggowitzer, G. Song, and A. Atrens, *Corros. Sci.*, 52 3687–3701 (2010).
34. H. R. Bakhsheshi-Rad, M. R. Abdul-Kadir, M. H. Idris, and S. Farahany, *Corros. Sci.*, 64 184–197 (2012).
35. X. N. Gu, W. Zheng, Y. Cheng, and Y. F. Zheng, *Acta Biomater.*, 5 2790–2799 (2009).
36. H. R. Bakhsheshi-Rad, E. Hamzah, M. Daroonparvar, M. Kasiri-Asgarani, and M. Medraj, *Ceram. Int.*, 40 14009–14018 (2014).